Correction

PHYSIOLOGY

Correction for "Arrhythmogenic late Ca^{2+} sparks in failing heart cells and their control by action potential configuration," by Ewan D. Fowler, Nan Wang, Melanie Hezzell, Guillaume Chanoit, Jules C. Hancox, and Mark B. Cannell, which was first published January 22, 2020; 10.1073/pnas.1918649117 (*Proc. Natl. Acad. Sci. U.S.A.* **117**, 2687–2692).

The authors note that the following statement should be added to the Acknowledgments: "The authors acknowledge funding from Medical Research Council UK Program Grant MR/N002903/1."

First published July 20, 2020.

www.pnas.org/cgi/doi/10.1073/pnas.2013263117

Arrhythmogenic late Ca^{2+} sparks in failing heart cells and their control by action potential configuration

Ewan D. Fowler[a], Nan Wang[a], Melanie Hezzell[b], Guillaume Chanoit[b], Jules C. Hancox[a], and Mark B. Cannell[a,1]

[a]School of Physiology, Pharmacology and Neuroscience, Faculty of Biomedical Sciences, University of Bristol, University Walk, BS8 1TD Bristol, United Kingdom; and [b]Bristol Veterinary School, University of Bristol, BS40 5DU Bristol, United Kingdom

Edited by Mark T. Nelson, University of Vermont, Burlington, VT, and approved December 24, 2019 (received for review October 24, 2019)

Sudden death in heart failure patients is a major clinical problem worldwide, but it is unclear how arrhythmogenic early afterdepolarizations (EADs) are triggered in failing heart cells. To examine EAD initiation, high-sensitivity intracellular Ca^{2+} measurements were combined with action potential voltage clamp techniques in a physiologically relevant heart failure model. In failing cells, the loss of Ca^{2+} release synchrony at the start of the action potential leads to an increase in number of microscopic intracellular Ca^{2+} release events ("late" Ca^{2+} sparks) during phase 2–3 of the action potential. These late Ca^{2+} sparks prolong the Ca^{2+} transient that activates contraction and can trigger propagating microscopic Ca^{2+} ripples, larger macroscopic Ca^{2+} waves, and EADs. Modification of the action potential to include steps to different potentials revealed the amount of current generated by these late Ca^{2+} sparks and their (subsequent) spatiotemporal summation into Ca^{2+} ripples/waves. Comparison of this current to the net current that causes action potential repolarization shows that late Ca^{2+} sparks provide a mechanism for EAD initiation. Computer simulations confirmed that this forms the basis of a strong oscillatory positive feedback system that can act in parallel with other purely voltage-dependent ionic mechanisms for EAD initiation. In failing heart cells, restoration of the action potential to a nonfailing phase 1 configuration improved the synchrony of excitation–contraction coupling, increased Ca^{2+} transient amplitude, and suppressed late Ca^{2+} sparks. Therapeutic control of late Ca^{2+} spark activity may provide an additional approach for treating heart failure and reduce the risk for sudden cardiac death.

heart | arrhythmia | cardiac myocytes | action potential | Ca^{2+} sparks

Worldwide, ~26 million people suffer from heart failure (HF) (1). More than 50% of HF patients die suddenly, and this sudden cardiac death is most likely due to the spontaneous emergence of arrhythmias (2, 3). At the cellular level, two identified initiators of cardiac arrhythmias are delayed afterdepolarizations (DADs) and early afterdepolarizations (EADs) (4). DADs occur in the resting period between heart beats (diastole) and are due to spontaneous Ca^{2+} release from the sarcoplasmic reticulum (SR) in the form of Ca^{2+} sparks (5), which summate to form propagating Ca^{2+}waves (6, 7). These waves cause a depolarizing inward current via the Na^{+}/Ca^{2+} exchange (NCX) mechanism (6, 8, 9). In contrast to DADs, EADs are less well understood and occur during the repolarization phase of the cardiac action potential (AP) where several ionic currents interact to control repolarization (10). EADs can be produced by reactivation of ionic currents during AP repolarization when the potassium currents forming the "repolarization reserve" (11, 12) are insufficient to maintain the repolarization trajectory of the AP, although why this should occur spontaneously within a steady train of APs is uncertain (13). Spontaneous Ca^{2+} waves have also been implicated in EAD generation (9), but it is unclear how such waves might be initiated when the SR should be depleted and/or refractory after SR Ca^{2+} release is triggered by the upstroke of the AP (14).

We recently showed that "late" Ca^{2+} sparks (LCS) can occur during the decay of the Ca^{2+} transient in normal rabbit cardiac myocytes (15). Here, we report that stochastic LCS and low-amplitude "Ca^{2+} ripples" are promoted in HF and can generate sufficient NCX current (I_{NCX}) to trigger EADs. In addition, normalizing the early AP waveform in HF promotes a faster and larger SR Ca^{2+} release (which should improve contractility) and at the same time decreases arrhythmogenic LCS activity.

Results

LCS occur in a wide variety of species (*SI Appendix*, Fig. S1), but, to study repolarization mechanisms, an AP similar to human is desirable, and we therefore used an established rabbit model of chronic myocardial infarction that causes HF. When left ventricular ejection fraction had fallen to 44 ± 3% (*SI Appendix*, Fig. S2 and Table S1), indicative of moderate to severe HF, ventricular myocytes exhibited t-tubule remodeling (Fig. 1 *A* and *B*) similar to that seen in most models of HF (16). This "t-tubule disease" (17) decreases the efficiency of excitation–contraction coupling and the rate of rise of the Ca^{2+} transient (*SI Appendix*, Fig. S3) (18, 19). Although there was no change in I_{Ca} density (Fig. 1*C*) in this HF model, the AP lost phase 1 repolarization (red arrow, Fig. 1*D*) and became prolonged (*SI Appendix*, Fig. S3). All of these changes are also seen in human HF (17, 20). The loss of AP phase 1 contributes to the reduced SR Ca^{2+} release rate (Fig. 1*E* and *SI Appendix*, Fig. S3) and increased SR release latency (Fig. 1*F*) (16, 18) because this phase of the AP affects the magnitude and time course of I_{Ca} which triggers SR Ca^{2+} release (21, 22).

Significance

Sudden cardiac death in heart failure is a major unsolved clinical problem that is linked to the development of a spontaneous arrhythmia. Early afterdepolarizations (EADs) are an arrhythmogenic mechanism, but the cellular trigger for EADs in heart failure is unclear. We show that the reduction in synchronous Ca^{2+} release early in the action potential (AP) of failing cardiac myocytes promotes the appearance of late Ca^{2+} sparks which can propagate, forming Ca^{2+} ripples and waves. These, in turn, produce an inward sodium–calcium exchange current which opposes AP repolarization. Restoration of AP phase 1 repolarization improved Ca^{2+} release synchrony and reduced late Ca^{2+} spark rate, suggesting a different approach to reducing the risk of sudden death in heart failure.

Author contributions: J.C.H. and M.B.C. designed research; E.D.F., N.W., M.H., and G.C. performed research; E.D.F., N.W., and M.B.C. analyzed data; E.D.F., J.C.H., and M.B.C. wrote the paper; and J.C.H. and M.B.C. assisted with funding acquisition.

The authors declare no competing interest.

This article is a PNAS Direct Submission.

[1]To whom correspondence may be addressed. Email: mark.cannell@bristol.ac.uk.

This article contains supporting information online at https://www.pnas.org/lookup/suppl/doi:10.1073/pnas.1918649117/-/DCSupplemental.

First published January 22, 2020.

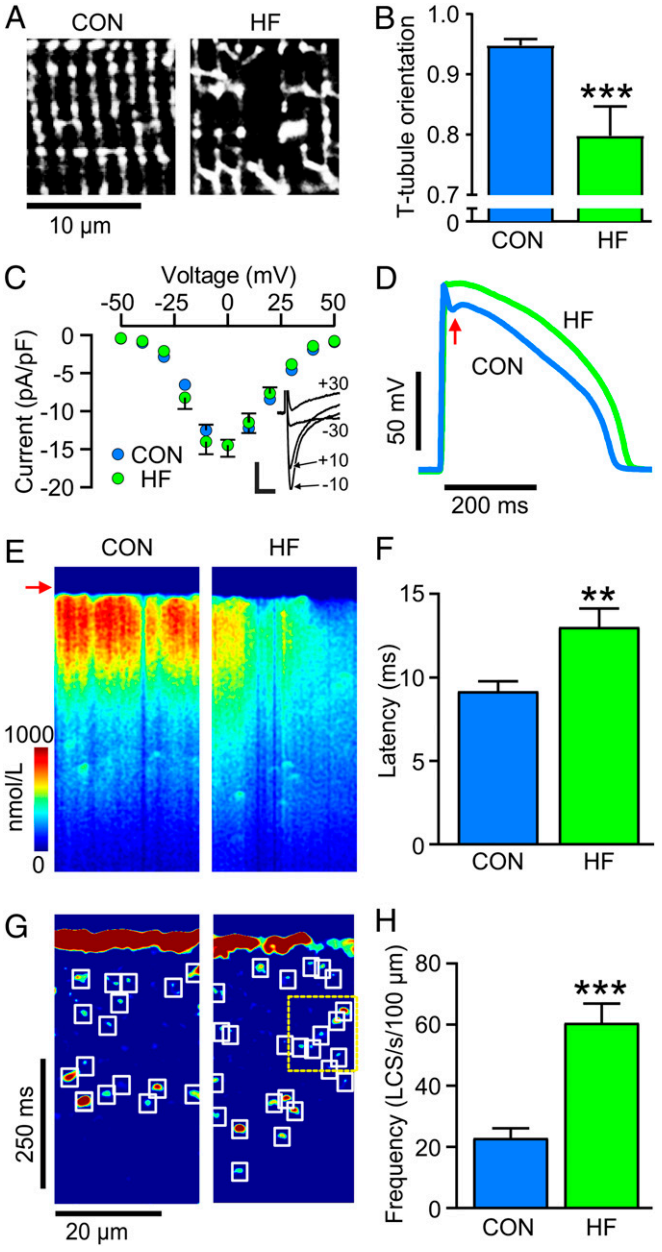

Fig. 1. Changes in structure, AP time course, t-tubule morphology, and increased LCS in HF. (*A*) di-8-ANEPPS staining shows reduced tubule regularity and (*B*) reorientation of t-tubules in HF cells compared to control (CON). *n*/*N* = 9/4 CON 12/5 HF. (*C*) I_{Ca} density was unchanged in HF. *n*/*N* = 20/4 CON 10/3 HF Representative currents at the indicated test potentials (mV) are shown (*Inset*). Error bars not shown where error is less than the size of symbols. (Scale bars: 5 pA/pF, 10 ms.) (*D*) APs in HF myocytes had less AP phase 1 repolarization (arrow). (*E*) Ca^{2+} transients in CON myocytes showed synchronous Ca^{2+} release, while HF showed less uniform Ca^{2+} release and (*F*) an increase in latency from electrical stimulation to detectable Ca^{2+} increase. (*G*) Image processing reveals increased LCS frequency in HF with some Ca^{2+} ripples (yellow dashed box). (*H*) LCS frequency was greater in HF cells than in CON. *n*/*N* = 16/6 CON; 14/5 HF. $^{**}P < 0.01$, $^{***}P < 0.001$, unpaired *t* tests.

The reduction in synchronous Ca^{2+} release in HF, seen as a less uniform increase in Ca^{2+} after the AP upstroke (Fig. 1*E*, arrow), was associated with an increase in the number of LCS (Fig. 1 *G* and *H*). This ~3-fold increase in LCS frequency can be explained by an increase in the number of Ca^{2+} release sites that were not triggered earlier during the AP (15, 22). The increased availability of Ca^{2+} release sites also promotes sequential activation of LCS, resulting in Ca^{2+} ripples (15), an example of which can be seen within the yellow dashed box in Fig. 1*G*.

Linkage between LCS and Arrhythmogenesis. LCS activity depends on SR Ca^{2+} content (15) which generally increases with AP frequency (10, 23). A pacing-pause protocol increases SR Ca^{2+} and may provoke EADs (24). With this protocol, LCS activity increased, and EADs appeared (Fig. 2*A*). The high rate of LCS production (and appearance of Ca^{2+} ripples; see *SI Appendix*, Fig. S4) in these conditions clearly opposed the normal decline of Ca^{2+} during the Ca^{2+} transient.

In order to generate an EAD, the net cellular repolarizing current (I_{net}) and/or repolarization reserve (11, 12) must be decreased and/or counteracted by depolarizing membrane current. While I_{net} is the sum of all inward and outward currents, the rate of change of membrane potential (dV_m/dt) is directly proportional to I_{net} because $I_{net} = -C_m \cdot dV_m/dt$ (where C_m is membrane capacitance). Applying this equation allows us to determine how much current is responsible for the repolarization phase of the AP, and Fig. 2*B* illustrates the magnitude and time course of I_{net}. In this exemplar, I_{net} was only ~0.18 pA/pF during the late AP repolarization phase, and the average I_{net} during AP repolarization was 0.26 ± 0.08 pA/pF (mean ± SD *n*/*N* = 15/4), showing that a small change in membrane currents will affect repolarization trajectory. It follows that any additional inward current of similar amplitude to I_{net} could stop AP repolarization (*SI Appendix*, Fig. S5) and thereby initiate an EAD.

An increase in intracellular Ca^{2+} moves the electrochemical gradient for NCX Ca^{2+} transport outward, causing an inward shift of I_{NCX} (25) which can be up to ~1 pA/pF in magnitude (26). To examine whether the observed LCS activity could produce sufficient I_{NCX} to oppose I_{net}, we voltage-clamped cells with a failing AP which included steps to different holding potentials around the times (and V_m) where EADs occur (Fig. 2*C*). During these V_m steps, many LCS occurred which triggered Ca^{2+} ripples and Ca^{2+} waves. The average Ca^{2+} (blue trace) and evoked inward current (black trace) are shown in Fig. 2 *D*, *Lower*. This inward current had a linear relationship to mean Ca^{2+} with a slope of −1.5 pA/pF/μmol/L (*SI Appendix*, Fig. S6), compatible with the expected Ca^{2+} dependence of I_{NCX} (26). The critical inward current (from Fig. 2*B*) that will balance I_{net} and stop repolarization is indicated by the dotted line which, after projection onto the Ca^{2+} records, reveals the Ca^{2+} changes associated with this critical current density. It is notable that this current density is developed just before the onset of Ca^{2+} waves which appear as chevron patterns in line scans (5, 7), showing that LCS and/or Ca^{2+} ripples can be the initiating events for EADs.

Fig. 2*E* shows that multiple Ca^{2+} ripples, rather than Ca^{2+} waves, can also give rise to EADs in current-clamped cells. In this exemplar, the line scan Ca^{2+}image (upper panel) is rather chaotic with no obvious Ca^{2+} waves being present. However, after image processing, numerous LCS events are seen, some of which form propagating Ca^{2+} ripples (cf. *SI Appendix*, Fig. S4). V_m and I_{net} can be linked to Ca^{2+} by two mechanisms: (1) Either Ca^{2+} activates inward I_{NCX} producing an inward shift of I_{net} and depolarization of V_m or (2) V_m activates L-type Ca^{2+} channels (LTCCs) which then trigger SR Ca^{2+} release. As shown by the colored bars in Fig. 2*E*, the rise in Ca^{2+} occurred in synchrony with inward I_{net} (peak value ~ 0.15 pA/pF) which also supports the idea that the initiation of EADs can result from the summation of LCS and Ca^{2+} ripples which activate inward I_{NCX}.

Model Analysis of the Role of I_{Ca} and I_{NCX} in EADs. The importance of I_{NCX} for EAD generation has also been demonstrated in murine cells by heterozygous NCX knockdown and in failing rabbit ventricle by acute NCX blockade (27, 28). To further test the idea that sufficient I_{NCX} can be generated by LCS to trigger an

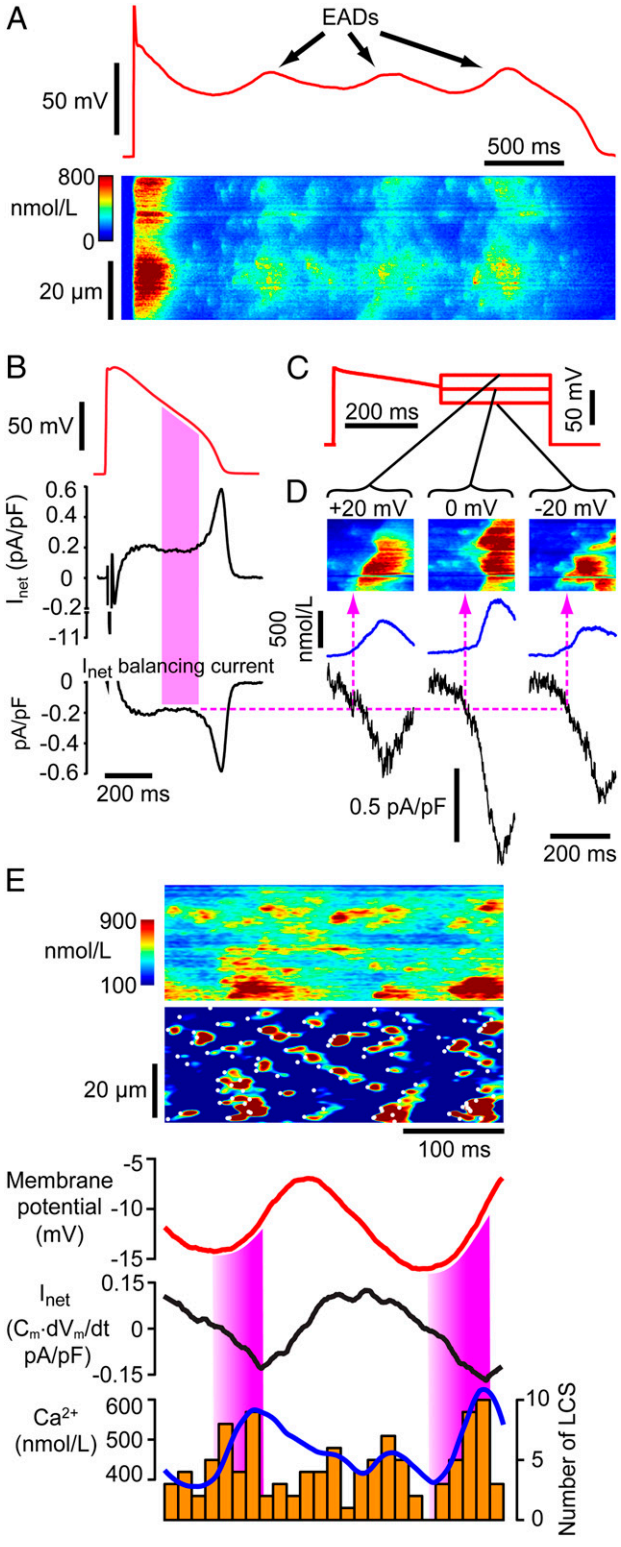

Fig. 2. LCS can trigger EADs. (*A*) EADs evoked by pacing-pause protocol. During repolarization, an initial V_m inflection at ~ −20 mV generates EADs (*Top*), and numerous LCS create oscillatory Ca^{2+} release (*Bottom*). (*B*) Calculation of I_{net} for a typical HF AP. The filled region indicates where the greatest number of LCS occur (*A* and Fig. 4*E*) and corresponds to an I_{net} of ~0.18 pA/pF. Any balancing current that counteracts I_{net} (i.e., $-I_{net}$, *Bottom*) will stop repolarization (*SI Appendix*, Fig. S5). (*C*) Failing AP with voltage-clamp steps used to probe Ca^{2+} and currents underlying EADs. (*D*) During the AP steps, LCS-triggered Ca^{2+} waves (*Top*) and inward currents (black trace) appear. Dashed line shows the inward current that balances I_{net} in *B* and could therefore stop repolarization. This current occurs when LCS are about to initiate Ca^{2+} waves. (*E*) Example of apparently chaotic Ca^{2+} during EADs in an HF cell (*Top*). Image processing reveals many LCS and Ca^{2+} ripples during V_m oscillations (red trace). The filled regions show where the depolarizing current (I_{net}) is increasing, and this corresponds to increasing Ca^{2+} (blue) and LCS activity (orange bars).

oscillatory EAD, we modified a new computer model of spatially distributed Ca^{2+} signaling (29) to calculate membrane currents that should occur in response to experimental V_m and Ca^{2+} signals (Fig. 3*A*). This approach breaks the intrinsic feedback loop(s) that otherwise make experimental dissection of causation problematic. Utilizing the recorded Ca^{2+} and V_m data shown in Fig. 2 as exemplar controlling variables, the model exhibited two types of behavior: when Ca^{2+} and LCS activity was high (Fig. 3*Ai*), I_{NCX} was in phase with dV/dt and of sufficient magnitude to explain the start of the V_m oscillations (cf. Fig. 2 *D* and *E*). However, when SR Ca^{2+} release was slightly reduced, changes in I_{NCX} were much smaller because the change in V_m opposed the change in electrochemical gradient for Ca^{2+} extrusion by NCX (Fig. 3*Aii*). The relative roles of I_{NCX} and I_{Ca} in initiating the EAD can be examined by cross-correlation with V_m. The magnitude of the negative peak in the cross-correlogram shows the strength of the linkage between these inward currents and V_m, while the time delay associated with the peak in the correlogram indicates whether they are the consequence of a change in V_m (by lagging behind V_m) or a potential cause (by leading the change in V_m). When the Ca load was high, inward I_{NCX} clearly preceded the change in V_m (Fig. 3*Bi*), consistent with the idea that the EADs were triggered by LCS activity and the consequent change in I_{NCX}. In comparison, I_{Ca} was both more weakly correlated and almost in phase with V_m. When SR load was decreased, the reduction in LCS activity led to a smaller inward I_{NCX} being less well correlated with V_m and with inappropriate phase to explain EAD initiation (Fig. 3*Bii*). However, I_{Ca} became more strongly correlated with V_m (due to a decrease in Ca^{2+}-dependent LTCC inactivation (10)) and had appropriate timing to explain EAD initiation. Thus, while both mechanisms for EAD generation were present in the model, an increase in Ca^{2+} release caused the dominant inward current trigger for EAD generation to shift from I_{Ca} reactivation to LCS-evoked I_{NCX}.

Improving Ca^{2+} Signaling and Suppressing LCS in HF Cells. Fig. 4*A* shows that a normal AP applied to HF cells increased the rate of rise and amplitude of the Ca^{2+} transient, and this was associated with an increase in Ca^{2+} release synchrony. On average, the normal AP increased the rate of rise of the Ca^{2+} transient from 30 ± 8 nmol/L/ms to 40 ± 9 nmol/L/ms ($P < 0.01$, paired *t* test), while the time to peak decreased from 75 ± 9 ms to 65 ± 9 ms ($P < 0.01$, paired *t* test). This improvement in excitation–contraction coupling efficiency was also reflected by a decrease in the latency for Ca^{2+} release (Fig. 4*B*). With the improvement in synchrony of early release, the duration of the Ca^{2+} transient became shorter (Fig. 4*C*) due to an ~50% decrease in LCS frequency (Fig. 4 *D* and *E*). These results confirm that at least a part of the nonuniform and delayed SR Ca^{2+} release seen in the HF model is due to AP phase 1 effects on I_{Ca}.

It may not be possible to completely restore the maximum rate of rise, time to peak Ca^{2+}, and Ca^{2+} transient duration to CON values with phase 1 modification alone because (1) the t-tubule disruption associated with HF would still be present and (2) there is reduced SERCA2a expression in HF which decreases SR Ca^{2+} uptake rate (30). Nevertheless, it is apparent that AP restoration can improve the defective Ca^{2+} signaling seen in HF and, importantly, reduce the LCS activity that can trigger EADs.

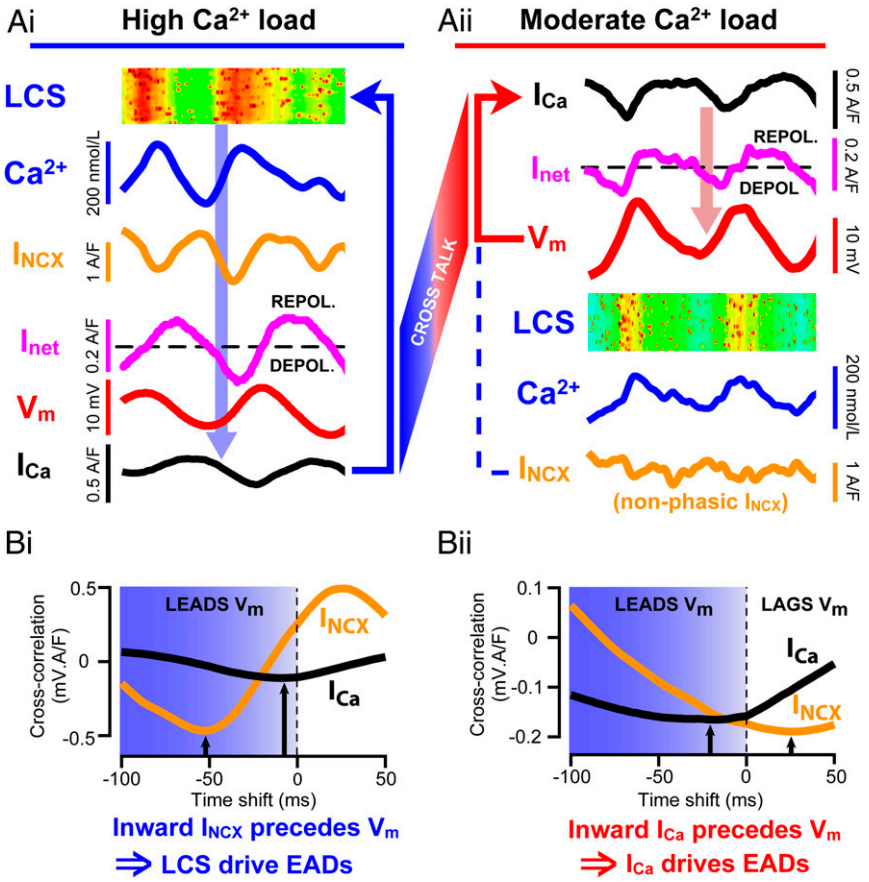

Fig. 3. Computer simulations of experimental traces using a model that generates LCS (29). Panels are ordered to indicate the flow of causation. (*Ai*) Increased LCS frequency is in phase with inward I_{NCX} and dV_m/dt, which precedes V_m and I_{Ca} forming an oscillatory feedback pathway as shown by the arrows. (*Aii*) When Ca^{2+} load is reduced, V_m oscillates because I_{Ca} (and possibly I_{Na}) supply the inward current to increase dV_m/dt and cause the EAD, as shown. In this case, LCS (and Ca^{2+}) are the consequence of the reactivation of I_{Ca}. Note that in this simulation, I_{NCX} bears no obvious relation to dV_m/dt (unlike the results shown in *Ai*). Cross-talk between the oscillators shown in *Ai* and *Aii* can occur because they contain common mechanisms. (*B*) Cross-correlograms between V_m and both I_{Ca} and I_{NCX} from the data shown in part A. The negative peaks in the cross-correlogram (black arrows) reveal both the strength of association (amplitude) and temporal relationship (offset from V_m) between V_m and I_{Ca} or $I_{NC}X$ (see *SI Appendix*). (*Bi*) When Ca^{2+} load was high, inward I_{NCX} preceded V_m oscillations and was more strongly correlated with V_m than I_{Ca}. (*Bii*) Under reduced Ca^{2+} load, I_{NCX} lags behind V_m oscillations. I_{Ca} reactivation preceded V_m and so has the required temporal relationship to explain EAD initiation, although some inward I_{NCX} may still contribute (13).

Discussion

Reactivation of I_{Ca} and I_{Na} to overcome the repolarization reserve and initiate EADs has been widely considered to be the primary mechanism for EAD generation (illustrated by the inner feedback loop shown in Fig. 5), e.g., refs. 11, 31, and 32. Indeed, when SR Ca^{2+} release was inhibited by blocking LTCCs, it was still possible to evoke EADs by a simulated I_{Ca} (33). Here we show that LCS-activated inward NCX current can initiate EADs and, we suggest, act as a coupled oscillator to further increase the risk for development of multiple EADs (outer loop in Fig. 5). This Ca^{2+} oscillator arises from two connected mechanisms: (1) Diffusion of Ca^{2+} from an initiating LCS may trigger additional LCS due to the gain inherent in Ca^{2+}-induced Ca^{2+} release (CICR). This SR load-dependent process manifests as propagating Ca^{2+} ripples and, if enough LCS sites are available, more synchronous and larger Ca^{2+} waves. (2) LCS will increase inward NCX current to depolarize V_m (34) while V_m couples back onto LCS activity via the V_m dependence of LTCC gating (which may explain the V_m dependence of LCS frequency shown in Fig. 4*E*). The stochastic nature of LCS provides an explanation for the sudden appearance of arrhythmogenic EADs, and, once started, an EAD will promote additional LCS and EADs due to the increased SR Ca^{2+} load arising from I_{Ca} reactivation.

The computer model clearly showed that both the electrical (V_m) and Ca^{2+} oscillators can couple and synergize (Fig. 4*A*). While the phase relationship between LCS-dependent NCX currents and dV_m/dt directly supports the idea that I_{NCX} can initiate Ca^{2+} dominant oscillations, I_{Ca} reactivation is also important (35) because late LTCC openings are a potent trigger for LCS (15). However, when Ca^{2+} levels are lower, and Ca^{2+} ripples and waves cannot form, EADs can still arise from instability in the repolarization process due to recruitment of noninactivated inward currents in the presence of insufficient repolarization reserve (11). In the latter case, smaller numbers of LCS may still play a lesser role in EAD initiation, and this is reminiscent of the role played by diastolic Ca^{2+} sparks in cardiac pacemaking by sino-atrial node cells (36).

Ca^{2+} Ripples, Ca^{2+} Waves, and V_m Oscillator Coupling. Although Ca^{2+} waves (Fig. 2*D*) have been implicated in EAD genesis (37), it is notable that the fluctuations in Ca^{2+} shown in Fig. 2 *A* and *E* are not typical Ca^{2+} waves (as seen in Fig. 2*D*) (6, 7); instead, the Ca^{2+} fluctuations came from low-amplitude Ca^{2+} ripples. In such cases, the local propagation of Ca^{2+} release (short-range Ca^{2+} ripples) may not be able to initiate cell-wide Ca^{2+} waves because the effective amplification of Ca^{2+} release by CICR is insufficient for full Ca^{2+} wave support. This lack of sufficient amplification

could be explained by the stochastic nature of LCS, coupled with local SR refractoriness (15, 38), decreasing the recruitment of adjacent LCS sites. Nevertheless, some synchronization in Ca^{2+} ripple initiation must occur for average Ca^{2+} to oscillate. The mathematical basis for the emergence of macroscopic Ca^{2+} oscillations from large numbers of independent LCS oscillators is beyond the scope of this study, but Kuramoto model analysis has shown that macroscopic oscillations can develop even when coupling across individual oscillators is weak (39). The relative importance of the Ca^{2+} and V_m oscillators in EAD generation will be variable because they depend on many factors such as the actual V_m trajectory, K^+ current availability, the level of SR Ca^{2+} loading in the cell, and I_{Ca} availability, as well as RYR2 Ca^{2+} sensitivity, as illustrated in Fig. 5. In connection with this point, increased LTCC activity and SR load associated with β-adrenergic stimulation (10) would almost certainly increase the risk for LCS-stimulated EADs.

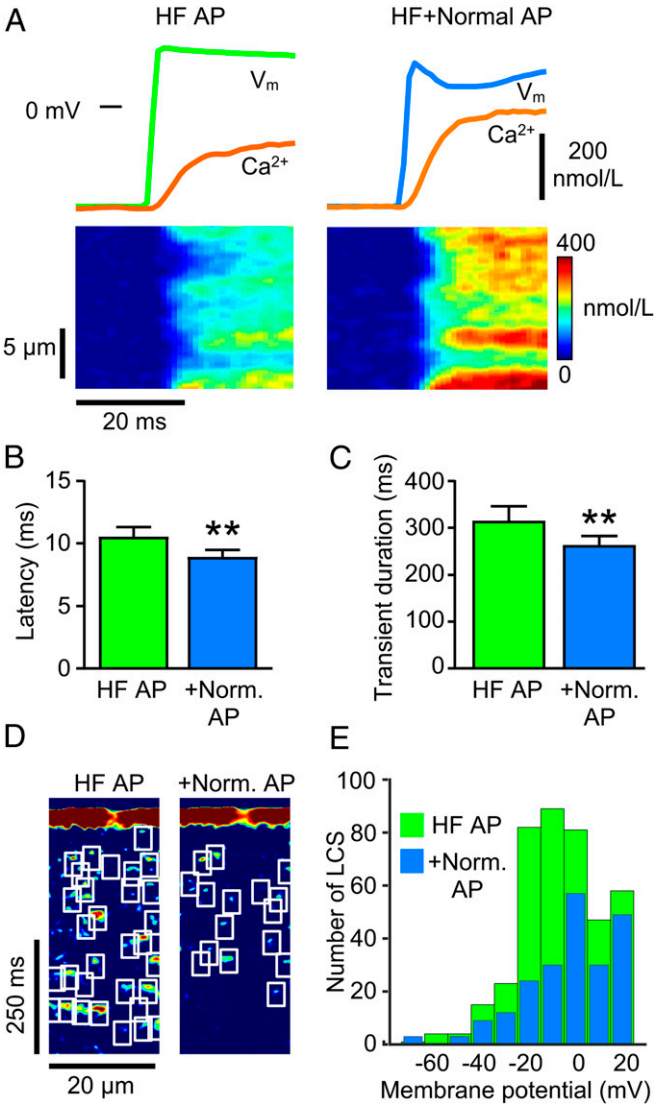

Fig. 4. Applying a normal AP to HF cells improves excitation–contraction coupling and reduces LCS frequency. (*A*) Ca^{2+} transient upstroke velocity, amplitude (orange), and Ca^{2+} release synchrony all increase in an HF cell (*Left*) when voltage-clamped with a normal AP (*Right*). (*Lower*) Improved synchrony in Ca^{2+} release. (*B*) Mean latency for Ca^{2+} release and (*C*) Ca^{2+} transient duration were reduced in HF cells clamped with a normal AP. (*D*) Processed Ca^{2+} images show fewer LCS in HF after applying normal AP. (*E*) Number of LCS detected in HF with failing AP waveform (HF AP, 404 LCS) and with a normal AP (+Norm AP, 217 LCS) from 13 HF cells binned by V_m during the AP repolarization. $^{**}P < 0.01$, paired *t* test *n*/*N* = 13/5.

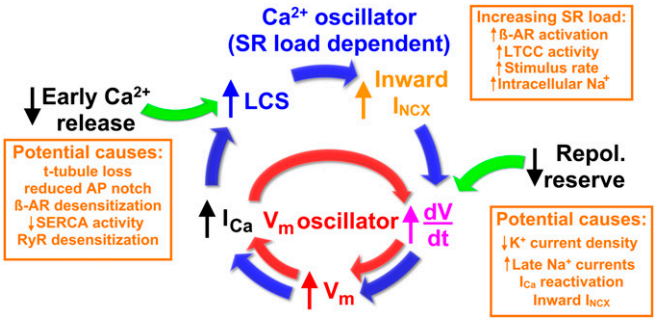

Fig. 5. Flow diagram for two interacting positive-feedback mechanisms that can drive V_m and Ca^{2+} oscillations during EADs. The red inner cycle represents the well-established V_m oscillator, wherein an increase in dV_m/dt (caused by a relative increase in depolarizing currents compared to repolarizing currents, e.g., text in orange box at *Lower Right*) leads to voltage-dependent reactivation of I_{Ca}, which in turn causes further depolarization. The blue outer cycle represents the stochastic LCS-mediated Ca^{2+} oscillator mechanism for EAD initiation. Reduced early Ca^{2+} release and/or increased SR load increases LCS production, and the resulting increase in inward I_{NCX} tends to depolarize the membrane which then feeds onto I_{Ca} to trigger additional LCS. Green arrows indicate possible factors contributing to EAD initiation. β-AR, beta-adrenoreceptor.

It should be noted that the LCS activity seen in our confocal line scans reflects only a small fraction of the actual number of LCS occurring in the entire cell; the confocal line scan surveys ∼2% of the cell volume, so ∼1 LCS/ms (Fig. 2*E*) would correspond to ∼50 LCS/ms cell-wide, and this much larger number underlies the measured NCX current that can initiate the EAD. This estimate is in reasonable agreement with the computer model used here which predicts that 107 LCS/ms may generate 0.26 pA/pF NCX current (29).

Since LTCC activity is common to both the V_m and Ca^{2+} oscillators, the idea that LTCC gating modification could be a therapeutic target for EAD prevention (33) becomes even more attractive. In addition, if modifying the late component of I_{Ca} is able to reduce net Ca^{2+} influx into the cell, SR Ca^{2+} content might be reduced (40), and this would also inhibit LCS activity (15). The improvement in Ca^{2+} signaling produced by applying a normal AP to HF myocytes is remarkable. This suggests that new therapies should be developed with the aim of improving early Ca^{2+} release by restoring phase 1 repolarization and/or restoring t-tubule regularity. This would reduce LCS frequency and thereby reduce the risk for potentially lethal LCS-triggered arrhythmias as well as mitigate the defective excitation–contraction coupling seen in HF (41).

Materials and Methods

More extensive details are available in *SI Appendix*. Briefly, all experiments were performed in accordance with the UK Home Office Animals (Scientific Procedures) Act 1986 and institutional approval by the University of Bristol ethics committee. We used an established coronary artery ligation model that leads to heart failure in adult New Zealand White rabbits (3–3.5 kg) which were daily monitored for health status. The target endpoint for HF was an ejection fraction of 40% (as measured by echocardiography *SI Appendix*, Fig. S2). Some rabbits did not quite reach this endpoint but presented other indicators of heart failure including dilated left ventricle and lung congestion (*SI Appendix*, Table S1). This model, due to repolarizing current behavior, can be used to gain insight into repolarization reserve with human relevance (42). It was not possible to wait for arrhythmias to start in this model (as they would be fatal), but EADs can be provoked in vitro by suitable interventions. Rather than use pharmacological manipulation to provoke EADs, we chose a pacing-pause method to minimize other possible perturbations of cellular function.

Cardiac Myocyte Isolation. Left ventricular epicardial myocytes were obtained from rabbit hearts after full anesthesia (50 mg/kg sodium pentobarbital i.v.) and euthanasia. Enzymatic dissociation was carried out using 1 mg/mL collagenase I (Worthington), 0.05 mg/mL protease (type XIV Sigma), and 0.1 mmol/L Ca^{2+}, as described previously (22). Guinea pig, rat, mouse, and zebrafish myocytes were isolated using similar methods to those described previously (22, 43, 44), and methods for zebrafish myocyte isolation are given in *SI Appendix*.

Electrophysiology. Electrophysiology experiments were performed in a modified Tyrode's solution (containing, in mmol/L: 133 NaCl, 5 KCl, 1 NaH_2PO_4, 10 4-(2-hydroxyethyl)-1-piperazineethanesulfonic acid (HEPES), 10 glucose, 1.8 $CaCl_2$, 1 $MgCl_2$, pH 7.4 with NaOH) at 36 ± 1 °C. Patch pipettes were pulled from borosilicate glass using a P80 micropipette puller (Sutter Instruments). Pipettes were filled with an intracellular solution containing, in mmol/L: 120 aspartic acid, 20 KCl, 10 HEPES, 10 NaCl, 5 glucose, 5 Mg.ATP, 0.05 Fluo-4 pentapotassium salt, with KOH added to adjust to pH 7.2. Tip resistance was typically 1.6–2.0 MΩ when filled with this solution. Membrane potential and currents were recorded using an Axopatch 1D amplifier (Molecular Devices), Power1401 digitizer (Cambridge Electronic Design), and Signal data acquisition software (version 6.04, Cambridge Electronic Design). Cell membrane capacitance was measured by step depolarizations to −75 mV from a holding potential of −80 mV for 25 ms. Series resistance was compensated by ∼70%. Liquid junction potential (10 mV) was subtracted from recordings.

Confocal Imaging. Ca^{2+} sparks and transients were recorded in line scan mode (45) from the fluo-4 loaded cells using an inverted confocal microscope (LSM 880, Zeiss) with a 1.4 NA 63× oil immersion lens. Excitation light was provided by a 488-nm argon laser, and fluorescence emission was collected at 492–600 nm. Ca^{2+} line scans were recorded with the pinhole set to <2 Airy units, at a pixel size of 0.1–0.2 μm/pixel, and with a scan speed of 1 ms per line. GaAsP photodetectors were used to increase the sensitivity of Ca^{2+} spark detection. The t-tubule system was imaged by labeling the sarcolemma with di-8-ANEPPS from a stock 1 mmol/L solution (in anhydrous dimethyl sulfoxide) added directly to the cell-recording chamber (final concentration 1 μmol/L) for 2–3 min. Excitation was at 488 nm, and emission was collected at >600 nm.

Statistical Analysis. Statistical analyses were performed at the level of the cell, and statistics on replicates of *n* individual independent cell experiments from *N* animals are given in the text as *n*/*N*. Data were tested for normality using the Shapiro-Wilk test (Prism7, Graphpad); in any cases where data were skewed, the test was reapplied to log-transformed data. Paired or unpaired *t* tests were performed on normally and log-normally distributed data. Results are presented as mean ± SEM. The limit of statistical confidence was $P < 0.05$.

Data Availability Statement. All data and computer codes are available upon request from the authors.

ACKNOWLEDGMENTS. We thank Drs. H. Cheng (BHF PG/16/55/32277 to J.C.H.), C. Du (BHF PG/15/106/31915 to J.C.H.), and R. J. Richardson for supplying some of the myocytes used for *SI Appendix*, Fig. S1 and Prof. G. L. Smith (University of Glasgow) for help and advice on HF model development.

1. P. Ponikowski *et al*., Heart failure: Preventing disease and death worldwide. *ESC Heart Fail.* **1**, 4–25 (2014).
2. E. J. Benjamin *et al*.; American Heart Association Council on Epidemiology and Prevention Statistics Committee and Stroke Statistics Subcommittee, Heart disease and stroke statistics-2019 update: A report from the American Heart Association. *Circulation* **139**, e56–e528 (2019).
3. G. F. Tomaselli, D. P. Zipes, What causes sudden death in heart failure? *Circ. Res.* **95**, 754–763 (2004).
4. W. T. Clusin, Calcium and cardiac arrhythmias: DADs, EADs, and alternans. *Crit. Rev. Clin. Lab. Sci.* **40**, 337–375 (2003).
5. H. Cheng, W. J. Lederer, M. B. Cannell, Calcium sparks: Elementary events underlying excitation-contraction coupling in heart muscle. *Science* **262**, 740–744 (1993).
6. J. R. Berlin, M. B. Cannell, W. J. Lederer, Cellular origins of the transient inward current in cardiac myocytes. Role of fluctuations and waves of elevated intracellular calcium. *Circ. Res.* **65**, 115–126 (1989).
7. H. Cheng, M. R. Lederer, W. J. Lederer, M. B. Cannell, Calcium sparks and $[Ca^{2+}]_i$ waves in cardiac myocytes. *Am. J. Physiol.* **270**, C148–C159 (1996).
8. S. R. Houser, V. Piacentino, 3rd, J. Weisser, Abnormalities of calcium cycling in the hypertrophied and failing heart. *J. Mol. Cell. Cardiol.* **32**, 1595–1607 (2000).
9. Y. Shiferaw, G. L. Aistrup, J. A. Wasserstrom, Intracellular Ca^{2+} waves, afterdepolarizations, and triggered arrhythmias. *Cardiovasc. Res.* **95**, 265–268 (2012).
10. D. M. Bers, *Excitation-Contraction Coupling and Cardiac Contractile Force* (Kluwer Academic Publishers, Dordrecht, ed. 2, 2001).
11. D. M. Roden, R. L. Abraham, Refining repolarization reserve. *Heart Rhythm* **8**, 1756–1757 (2011).
12. B. Hegyi *et al*., Altered repolarization reserve in failing rabbit ventricular myocytes: Calcium and β-adrenergic effects on delayed- and inward-rectifier potassium currents. *Circ. Arrhythm Electrophysiol.* **11**, e005852 (2018).
13. D. Sato, L.-H. Xie, T. P. Nguyen, J. N. Weiss, Z. Qu, Irregularly appearing early afterdepolarizations in cardiac myocytes: Random fluctuations or dynamical chaos? *Biophys. J.* **99**, 765–773 (2010).
14. E. A. Sobie, L.-S. Song, W. J. Lederer, Local recovery of Ca^{2+} release in rat ventricular myocytes. *J. Physiol.* **565**, 441–447 (2005).
15. E. D. Fowler, C. H. T. Kong, J. C. Hancox, M. B. Cannell, Late Ca^{2+} sparks and ripples during the systolic Ca^{2+} transient in heart muscle cells. *Circ. Res.* **122**, 473–478 (2018).
16. K. R. Sipido, H. Cheng, T-tubules and ryanodine receptor microdomains: On the road to translation. *Cardiovasc. Res.* **98**, 159–161 (2013).
17. D. J. Crossman *et al*., T-tubule disease: Relationship between t-tubule organization and regional contractile performance in human dilated cardiomyopathy. *J. Mol. Cell. Cardiol.* **84**, 170–178 (2015).
18. S. E. Litwin, D. Zhang, J. H. Bridge, Dyssynchronous Ca^{2+} sparks in myocytes from infarcted hearts. *Circ. Res.* **87**, 1040–1047 (2000).
19. L. S. Song *et al*., Orphaned ryanodine receptors in the failing heart. *Proc. Natl. Acad. Sci. U.S.A.* **103**, 4305–4310 (2006).
20. V. Piacentino, 3rd *et al*., Cellular basis of abnormal calcium transients of failing human ventricular myocytes. *Circ. Res.* **92**, 651–658 (2003).
21. R. Sah, R. J. Ramirez, P. H. Backx, Modulation of Ca^{2+} release in cardiac myocytes by changes in repolarization rate: Role of phase-1 action potential repolarization in excitation-contraction coupling. *Circ. Res.* **90**, 165–173 (2002).
22. P. J. Cooper, C. Soeller, M. B. Cannell, Excitation-contraction coupling in human heart failure examined by action potential clamp in rat cardiac myocytes. *J. Mol. Cell. Cardiol.* **49**, 911–917 (2010).
23. M. Endoh, Force-frequency relationship in intact mammalian ventricular myocardium: Physiological and pathophysiological relevance. *Eur. J. Pharmacol.* **500**, 73–86 (2004).
24. P. C. Viswanathan, Y. Rudy, Pause induced early afterdepolarizations in the long QT syndrome: A simulation study. *Cardiovasc. Res.* **42**, 530–542 (1999).
25. D. A. Eisner, W. J. Lederer, Na-Ca exchange: Stoichiometry and electrogenicity. *Am. J. Physiol.* **248**, C189–C202 (1985).
26. K. S. Ginsburg, C. R. Weber, D. M. Bers, Cardiac Na^+-Ca^{2+} exchanger: Dynamics of Ca2+-dependent activation and deactivation in intact myocytes. *J. Physiol.* **591**, 2067–2086 (2013).
27. N. Bögeholz *et al*., Suppression of early and late afterdepolarizations by heterozygous knockout of the Na^+/Ca^{2+} exchanger in a murine model. *Circ. Arrhythm Electrophysiol.* **8**, 1210–1218 (2015).
28. P. Milberg *et al*., Acute inhibition of the Na^+/Ca^{2+} exchanger reduces proarrhythmia in an experimental model of chronic heart failure. *Heart Rhythm* **9**, 570–578 (2012).
29. M. Zhong *et al*., NCX-Mediated subcellular Ca^{2+} dynamics underlying early afterdepolarizations in LQT2 cardiomyocytes. *Biophys. J.* **115**, 1019–1032 (2018).
30. M. Flesch *et al*., Sarcoplasmic reticulum Ca^{2+}ATPase and phospholamban mRNA and protein levels in end-stage heart failure due to ischemic or dilated cardiomyopathy. *J. Mol. Med. (Berl.)* **74**, 321–332 (1996).
31. C. T. January, J. M. Riddle, Early afterdepolarizations: Mechanism of induction and block. A role for L-type Ca^{2+} current. *Circ. Res.* **64**, 977–990 (1989).
32. M. Boutjdir, N. el-Sherif, Pharmacological evaluation of early afterdepolarisations induced by sea anemone toxin (ATXII) in dog heart. *Cardiovasc. Res.* **25**, 815–819 (1991).
33. R. V. Madhvani *et al*., Shaping a new Ca^{2+} conductance to suppress early afterdepolarizations in cardiac myocytes. *J. Physiol.* **589**, 6081–6092 (2011).
34. D. Sato, R. E. Dixon, L. F. Santana, M. F. Navedo, A model for cooperative gating of L-type Ca^{2+} channels and its effects on cardiac alternans dynamics. *PLoS Comput. Biol.* **14**, e1005906 (2018).
35. J. N. Weiss, A. Garfinkel, H. S. Karagueuzian, P.-S. Chen, Z. Qu, Early afterdepolarizations and cardiac arrhythmias. *Heart Rhythm* **7**, 1891–1899 (2010).
36. V. A. Maltsev, E. G. Lakatta, Dynamic interactions of an intracellular Ca^{2+} clock and membrane ion channel clock underlie robust initiation and regulation of cardiac pacemaker function. *Cardiovasc. Res.* **77**, 274–284 (2008).
37. Z. Zhao *et al*., Revisiting the ionic mechanisms of early afterdepolarizations in cardiomyocytes: Predominant by Ca waves or Ca currents? *Am. J. Physiol. Heart Circ. Physiol.* **302**, H1636–H1644 (2012).
38. E. A. Sobie, W. J. Lederer, Dynamic local changes in sarcoplasmic reticulum calcium: Physiological and pathophysiological roles. *J. Mol. Cell. Cardiol.* **52**, 304–311 (2012).
39. B. Pietras, A. Daffertshofer, Network dynamics of coupled oscillators and phase reduction techniques. *Phys. Rep.* **819**, 1–105 (2019).
40. D. A. Eisner, H. S. Choi, M. E. Díaz, S. C. O'Neill, A. W. Trafford, Integrative analysis of calcium cycling in cardiac muscle. *Circ. Res.* **87**, 1087–1094 (2000).
41. A. M. Gómez *et al*., Defective excitation-contraction coupling in experimental cardiac hypertrophy and heart failure. *Science* **276**, 800–806 (1997).
42. I. Baczkó, N. Jost, L. Virág, Z. Bősze, A. Varró, Rabbit models as tools for preclinical cardiac electrophysiological safety testing: Importance of repolarization reserve. *Prog. Biophys. Mol. Biol.* **121**, 157–168 (2016).
43. S. M. Bryant *et al*., Caveolin 3-dependent loss of t-tubular I_{Ca} during hypertrophy and heart failure in mice. *Exp. Physiol.* **103**, 652–665 (2018).
44. H. Cheng *et al*., Potent hERG channel inhibition by sarizotan, an investigative treatment for Rett Syndrome. *J. Mol. Cell. Cardiol.* **135**, 22–30 (2019).
45. M. B. Cannell, H. Cheng, W. J. Lederer, Spatial non-uniformities in $[Ca^{2+}]_i$ during excitation-contraction coupling in cardiac myocytes. *Biophys. J.* **67**, 1942–1956 (1994).